Biosensors and Bioelectronics 169 (2020) 112613

Contents lists available at ScienceDirect

Biosensors and Bioelectronics

journal homepage: http://www.elsevier.com/locate/bios

Peptide-functionalized metal-organic framework nanocomposite for ultrasensitive detection of secreted protein acidic and rich in cysteine with practical application

Shuai Wu [a], Zhaowei Sun [a], Ying Peng [a], Yiwei Han [a], Jinlong Li [b], Sha Zhu [c], Yongmei Yin [c,**], Genxi Li [a,d,*]

[a] State Key Laboratory of Pharmaceutical Biotechnology, School of Life Sciences, Nanjing University, Nanjing, 210023, PR China
[b] Department of Laboratory Medicine, The Second Affiliated Hospital of Southeast University, Nanjing, 210003, PR China
[c] Department of Oncology, The First Affiliated Hospital of Nanjing Medical University, Nanjing, 210029, PR China
[d] Center for Molecular Recognition and Biosensing, School of Life Sciences, Shanghai University, Shanghai, 200444, PR China

ARTICLE INFO

Keywords:
Metal-organic frameworks
Enzyme catalysis
Peptide-functionalized nanocomposites
Secreted protein acidic and rich in cysteine
Clinical diagnostics

ABSTRACT

In this work, we have prepared peptide-functionalized metal-organic frameworks (MOFs) as signal-amplifying tags for the detection of secreted protein acidic and rich in cysteine (SPARC). Furthermore, enzyme-MOF nanocomposites are fabricated via a coprecipitation strategy between horse radish peroxidase (HRP) and ZIF-90, where ZIF-90 is used as a protective support for HRP immobilization. Meanwhile, the peptide sequence has been designed as SPARC-binding peptide, which imparts biorecognition functionality to HRP@ZIF-90 for performing a colorimetric sensor. Therefore, during the test, HRP molecules can be quickly released from nanocomposites by acidic condition to catalyze chromogenic reaction, enabling the ultrasensitive detection of SPARC with a low detection limit of 30 fg/mL. Moreover, the content of SPARC in colon cancer tissues with different degrees of differentiation can be determined with this sensor, demonstrating that the expression of SPARC is closely related to the occurrence, invasion and metastasis of human colon cancer. These results may show the potential applications of this biosensor in SPARC fundamental research as well as clinical diagnosis in the future.

1. Introduction

The development of malignancy is a complex pathological process (Hanahan and Weinberg, 2000, 2011). It is increasingly released that **this** process is closely associated with tumor microenvironment, which encompasses the extracellular matrix, surrounding stroma, fibroblasts, and signaling molecules (Joyce and Pollard, 2009; Junttila and de Sauvage, 2013; Quail and Joyce, 2013). Moreover, these intercellular communications at the cancer cell-microenvironment interface often occur at the protein level (Bornstein and Sage, 2002; Wong and Rustgi, 2013). For instance, secreted protein acidic and rich in cysteine (SPARC), a prototypic matricellular glycoprotein at the center of microenvironment network, can modulate cell–cell and cell–matrix interactions (Clark and Sage, 2008). The overexpression of SPARC has also been reported to be correlated with progression of various cancers including colon cancer (Liu and Hsiao, 2013), breast cancer (Ma et al., 2017), ovarian cancer (Said et al., 2008), and pancreatic cancer (Papapanagiotou et al., 2018). The characterization of SPARC level in tumor tissues may enhance understanding of fundamental tumor biology such as carcinogenesis, tumor progression, invasion, and metastasis, as well as provide novel preventive and therapeutic strategies for cancers. Therefore, accurate and sensitive assay methodology for detection of SPARC is highly required.

Enzyme-linked immunosorbent assay (ELISA) using enzyme-antibody conjugates is the main diagnostic tool for the measurement of SPARC (Tichet et al., 2015). However, as a practical matter, conventional ELISA has to be confronted with some challenges. Firstly, the biological activity of enzyme and antibody is very sensitive to environment interference. So, the relevant reagents must be transported at low temperatures, which certainly raises costs. Secondly, the coupled

* Corresponding author. State Key Laboratory of Pharmaceutical Biotechnology, School of Life Sciences, Nanjing University, Nanjing, 210023, PR China.
** Corresponding author.
E-mail addresses: ymyin@njmu.edu.cn (Y. Yin), genxili@nju.edu.cn (G. Li).

https://doi.org/10.1016/j.bios.2020.112613
Received 30 June 2020; Received in revised form 31 August 2020; Accepted 12 September 2020
Available online 15 September 2020

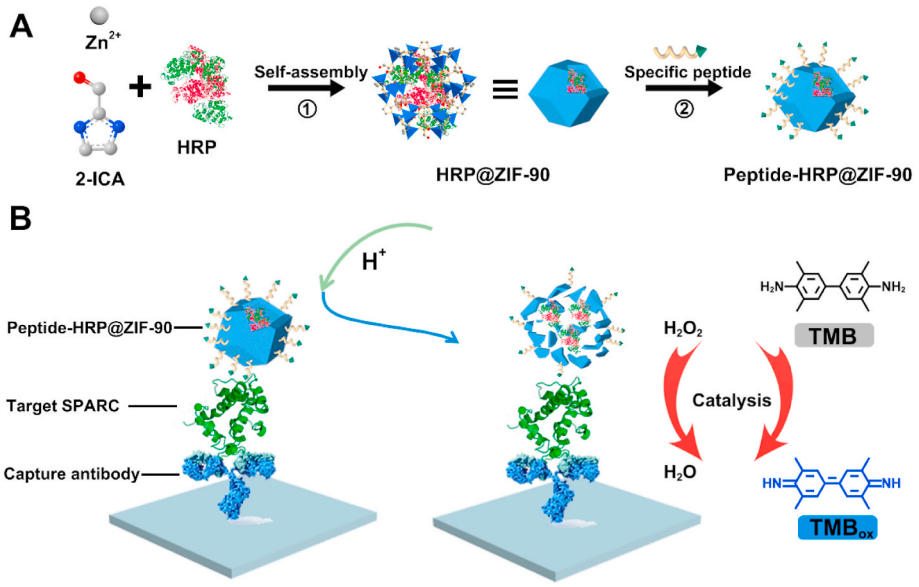

Scheme 1. Schematic diagram for (A) the fabrication process of peptide-HRP@ZIF-90 and (B) colorimetric detection of target SPARC.

reaction between enzyme and antibody suffers from a complex purification process and poor storage stability, which can easily lead to the inactivation of biological molecules. Thirdly, the detection performance cannot meet the requirements when using low biopsy samples due to its relatively low sensitivity. Currently, some other methods such as western blots, immunohistochemistry, and fluorescence in situ hybridization (FISH) have also been adopted for qualitative analysis of SPARC. Nevertheless, they are cumbersome and false negative easily. Therefore, a sensitive, reliable, and stable sensing platform to improve the stability of enzymes and amplify the signal for the detection of SPARC should be developed.

Metal-organic frameworks (MOFs) are crystalline and periodic networks constructed from inorganic nodes joined by organic linkers through coordination bonds, which have recently garnered immense attention in many applications, including gas storage (Li et al., 2009), catalysis (Sanati et al., 2020), environment protection (Abazari et al., 2020), energy conversion (Abazari et al., 2019b; Sanati et al., 2019), and an increasing amount of potential biomedical applications (Abazari et al., 2019a; Gimenez-Marques et al., 2016; Horcajada et al., 2012), due to their structural diversity, tunable porosity, and biocompatibility. Particularly, MOFs have been emerged as advantageous platforms for enzyme immobilization, producing novel enzyme-MOF composites (Drout et al., 2019; Huang et al., 2020; Lian et al., 2017). The large surface area and well-defined porosity of MOFs ensures that a large number of enzymes can be encapsulated with high loading efficiency. Besides, their robust framework architectures can provide thermostable and chemically shells for the encapsulated enzymes (Liang et al., 2015; Shieh et al., 2015). Thus, the formed enzyme-MOF composites often exhibit excellent stability and improved catalytic performance, which are very helpful for biosensing applications (Kou et al., 2020; Liang et al., 2019). Therefore, we hypothesized that these advanced composite materials may be able to overcome the shortages in conventional SPARC testing.

Herein, for the first time, we have prepared peptide-functionalized MOFs. Furthermore, enzyme-MOF nanocomposites are fabricated and applied for the specific and sensitive detection of SPARC with practical application in this work. The scheme has been shown in Scheme 1. Firstly, a classical crystalline ZIF structure (ZIF-90)

(Morris et al., 2008) using imidazolate-2-carboxyaldehyde (2-ICA) as organic ligand has been synthesized as exoskeleton to encapsulate horseradish peroxidase (HRP) via a self-assembly strategy, where the enzymes are encapsulated within the frameworks during the synthetic process. In such design, mild synthetic conditions are helpful to preserve the original activity of HRP. Meanwhile, ZIF-90 can shield HRP molecules with exceptional stability to resist external interference and provide a functional interface rich in the aldehyde group for post-modification. To realize specific molecular recognition, we have introduced the SPARC-binding peptides (NH_2-GGGSPPTGIN) to the surface of HRP@ZIF-90 via Schiff's base reaction between aldehyde group and N-terminal of peptides (Zhang et al., 2017), followed by the step of addition of $NaBH_4$ to reduce the formed imine group (Fig. S1). These peptides, which possess high specificity, good biocompatibility, and great stability, are screened from the random peptide library by using phage display technology (Ghosh et al., 2012; Kelly et al., 2006). The assembly of peptides on the external of HRP@ZIF-90 can construct a steric and electrostatic barrier to stabilize ZIF nanoparticles in biological environment and renders them functional with respect to molecular recognition for bioassays. Therefore, a colorimetric sensing method can be proposed using peptide-HRP@ZIF-90 as signal tags. After capturing the targets, the peptide-modified nanocomposites are then added, thus the HRP molecules can be quickly released from nanocomposites under acidic conditions and the substrate 3, 3′, 5, 5′-tetramethylbenzidine (TMB) is oxidized to give the colorimetric signal readout (Gao et al. 2015, 2017a, 2017b). Moreover, a large number of immobilized enzyme molecules ensure the signal amplification of this method, enabling ultrasensitive detection for SPARC. This method is also in favor of analysis of colon cancer tissue samples, which may provide an alternative tool for cancer diagnosis.

2. Experimental section

2.1. Reagents and apparatus

Full details are given in the Supporting Information section.

2.2. Synthesis of ZIF-90 and HRP@ZIF-90

ZIF-90 was synthesized as follows: zinc nitrate (15 mg) was added into deionized (DI) water (3 mL). Then, this solution was added to DI water (7 mL) containing imidazolate-2-carboxyaldehyde (192 mg), and polyvinyl pyrrolidone (20 mg). After mixing the solutions above, the resulting powder was stirred for a few minutes. All reactions were carried out at room temperature. Finally, the as-obtained products were collected by centrifugation (10500 rpm), washed with excess DI water,

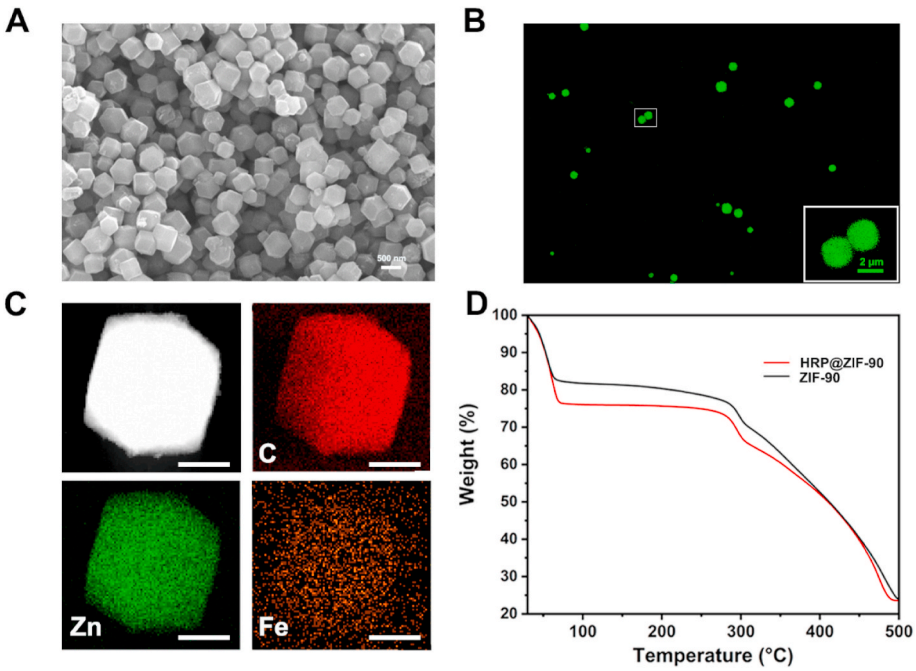

Fig. 1. (A) SEM images of HRP@ZIF-90. (B) Confocal microscope images of 2 μm FITC-HRP@ZIF-90 particles. (C) The corresponding elemental mapping of the HRP@ZIF-90. The scale bar is 200 nm. (D) TGA curves of ZIF-90 and HRP@ZIF-90 nanoparticles.

and vacuum dried at room temperature.

The synthesis of ZIF-90 nanoparticles was similar to the above method but with addition of HRP (2 mg).

2.3. Surface modification of HRP@ZIF-90

Firstly, 4 mg of HRP@ZIF-90 were placed into 500 μL methanol and sonicated for 3 min. Then 500 μL methanol solution containing 1 mg of peptide powder was added. Then the resulting mixture was placed on a shaker and shaken at room temperature for 12 h. MOFs-peptide conjugates were formed, and an excess number of free peptides was removed by centrifugation (10500 rpm, 5 min). Next, the solid were resuspended in 2 mL methanol and 1.8 mg of $NaBH_4$ were added into the solution under gentle shaking. After 1 h, the reaction products were collected by centrifugation (10500 rpm, 5 min) and dried under vacuum.

2.4. Colorimetric assay for SPARC

100 μL of the SPARC antibody solution (3 μg/mL) was added into each well of the microtiter plate. The plate was incubated at 4 °C overnight. After removing the solutions, the plate was washed with 0.05% Tween-20 in PBS buffer (PBST). Then 150 μL of blocking buffer were added into each well for 1 h at room temperature, followed by copious rinsing with PBST solutions for three times. After that, 100 μL of the PBST solutions containing different concentration of protein targets were added to the antibody-modified wells for 1 h at room temperature. The PBST-only solution was performed as the negative control. Then repeat washing steps for three runs. In a typical sandwich-type immunoassay, 100 μL of peptide-modified HRP@ZIF-90 (50 μg/mL) was diluted in Tris-HCl (20 mM, pH 8) containing 1% BSA into each well. The microtiter plate was covered with a sealer and incubated the at room temperature for 1 h with vigorous shaking. The next step, the unbound HRP@ZIF-90 was removed by PBST solutions for two times. Finally, 100 μL of TMB/H_2O_2 solution prepared by 2 mM TMB and 0.2 M H_2O_2 in tris-citric acid buffer was added into the microplate well. After incubation at room temperature for 15 min, 50 μL of stop buffer (1 M H_2SO_4) was added to terminate the reaction. The absorbance intensities were recorded by microplate reader at 450 nm.

2.5. Detection of SPARC in clinical tissue samples

Clinical tissue samples were collected from the Second Affiliated Hospital of Southeast University. Informed consents were obtained in all cases, and the research was approved by the scientific ethical committee of Nanjing University and Southeast University. The sections of tissues were prepared for staining and observation with clinical medical equipment. Additionally, we extracted the total protein from the fresh tissues of similar size using precooled extraction reagent (One Step Animal Tissue Active Protein Extraction Kit) and made them into the lysates. The following step of immunoassay was same with above method.

3. Results and discussions

3.1. Preparation and characterization of HRP@ZIF-90 nanocomposites

HRP is the commonly used enzyme in biological assay, which serves as catalytic labels for visual detection (Veitch, 2004). Thus, we have selected HRP as guests to prepare the HRP@ZIF-90 nanoparticles by directly mixing 2-ICA and Zn^{2+} in the presence of HRP at room temperature. Experimental results reveal that a higher ratio of the two precursors can effectively scale down the particle size of the resulting nanocomposites, but the yields of products also decrease accordingly at the same time. To maximize the effect, the ratio of 2-ICA and Zn^{2+} is set at 40:1, the size of the HRP@ZIF nanoparticles is around 400–600 nm with regular cubic morphology as characterized by scanning electron microscope (SEM) (Fig. 1A). To confirm that HRP is embedded in the cavity of ZIF-90 crystals, we have employed the fluorescein (FITC)--tagged HRP to determine the spatial distribution. Considering the resolution of confocal laser microscopy, larger particles (2 **μm**) have been prepared by changing the ratio to be 10:1. As shown in Fig. 1B, the colocalization of FITC is distributed within the ZIF-based nanocomposites. To further demonstrate the successful encapsulation of HRP in the MOFs, the energy dispersive X-ray spectroscopy (EDS) mapping of HRP@ZIF-90 is shown in Fig. 1C, the elements of C and Zn come from the frameworks of ZIF-90 and the existence of Fe element is due to the presence of heme groups in HRP enzyme. Also, the thermogravimetric

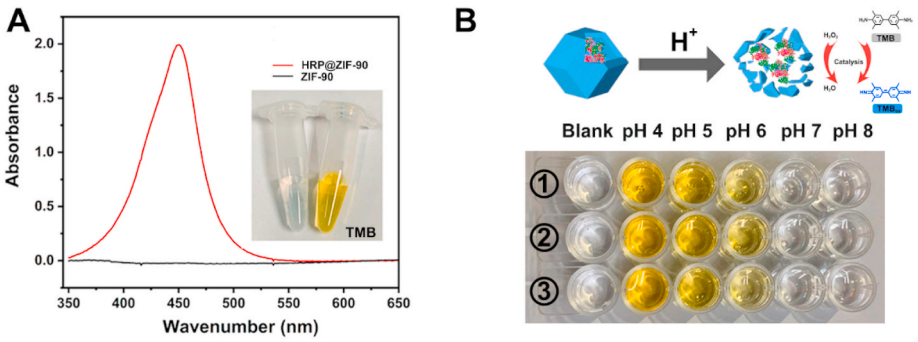

Fig. 2. (A) Results of chromogenic reaction catalyzed by ZIF-90 and HRP@ZIF-90 using TMB/H_2O_2 as substrate. (B) Schematic diagram for the catalytic mechanism and the chromogenic results catalyzed by HRP@ZIF-90 at different values.

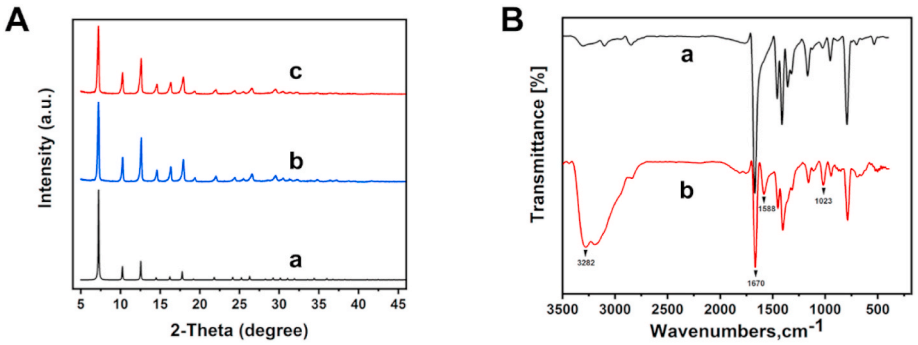

Fig. 3. (A) PXRD patterns of the crystal structure of (a) simulated ZIF-90, (b) as-synthesized HRP@ZIF-90, and (c) peptide-functionalized HRP@ZIF-90. (B) FT-IR spectra of (a) as-synthesized HRP@ZIF-90 and (b) peptide-HRP@ZIF-90.

analysis (TGA) of HRP@ZIF-90 and ZIF-90 (Fig. 1D) clearly verifies the existence of enzyme.

Then, we have studied the catalytic properties of HRP@ZIF-90. A commercial TMB chromogenic solution (pH 5.6) has been selected as substrate to test the catalytic activity of ZIF-90 and HRP@ZIF-90. As shown in Fig. 2A, the nanocomposites exhibit strong catalytic activity in TMB chromogenic reaction via measuring the ultraviolet spectrophotometer absorbance at 450 nm. But no measurable absorbance can be observed if using the pure ZIF-90 nanoparticles, implying that the embedded HRP molecules play the key roles in catalytic reaction. To further explain the mechanism of enzymatic reaction, we have prepared several solutions containing TMB/H_2O_2 at different pH values (pH 4–8). As shown in Fig. 2B, the results of three repeated experiments indicate that chromogenic reactions can occur only under acidic conditions.

Not under alkaline conditions. Thus, we hypothesized that the acid solution could destroy the skeleton of ZIF-90, releasing the HRP molecules from the inside. To test this, we have first employed SEM to observe the structure change of HRP@ZIF-90 at different pH values. As shown in Fig. S2, it can be observed that the structure of HRP@ZIF-90 collapsed under acidic conditions, but still maintained a relatively complete morphology under alkaline conditions. Meanwhile, we have conducted a contrast test between HRP@ZIF-90 and free HRP. As shown in Fig. S3, free HRP enzymes can catalyze reactions over a wide pH range with different biological activities, which suggests that the framework structure of ZIF-90 prevent the interaction between HRP and substrate indirectly. It's probably because that HRP are encapsulated through slow coprecipitation during the nucleation process of ZIF-90, the prepared HRP@ZIF-90 showed no catalytic activity under alkaline condition due to the unfolding effects and competing coordination caused by the imidazolate-2-carboxyaldehyde ligand (Chen et al., 2020; Wei et al., 2019). Moreover, the kinetics study shows that HRP@ZIF-

90 exhibits a slower rate of reaction than free HRP (Fig. S4), further demonstrating that the structure of ZIF-90 is gradually destroyed during the process.

To explore the chemical stability of the nanocomposites, HRP@ZIF-90 has been treated in several perturbation environments such as proteolytic agents or heating treatment. As shown in Fig. S5, the protected HRP recovered from HRP@ZIF-90 maintains high biocatalytic activity than free HRP under the same conditions, which benefits from the framework structure of ZIF-90, providing a protective coating for enzymes.

3.2. Characterization of peptide-functionalized HRP@ZIF-90

Then a post-synthetic procedure has been carried out to functionalize HRP@ZIF-90 crystals by introducing SAPRC-binding peptides with the Schiff's base reaction. As shown in Fig. 3A, HRP@ZIF-90 exhibits similar diffraction peaks with simulated ZIF-90 in powder X-ray diffraction (PXRD) patterns, suggesting that the prepared nanoparticles possess good purity and high crystallinity. What's more, the pattern of.

Peptide-functionalized HRP@ZIF-90 persists with little change, indicating the modification has no influence on its crystal structure. Transmission electron microscopy (TEM) image also shows its structural integrity (Fig. S6). Further insight into the surface modification has been achieved through Fourier transform infrared spectroscopy (FT-IR) analysis. The FI-TR spectrum of HRP@ZIF-90 is shown in Fig. 3B. The band at 1670 cm^{-1} in the HRP@ZIF-90 spectrum is ascribed to the C═O stretching frequency. The characteristic normal modes of vibration of the imidazole ring are consistent with those of the previous report (Yang and Chung, 2013). Upon modification with peptides, the intensity of the band at 1670 cm^{-1} has been decreased a bit but a new peak appears at 1588 cm^{-1}, which provides evidence for the presence of amide. At the same time, an improved intensity at 1203 cm^{-1} proves that imine has been reduced by $NaBH_4$ to generate C–N bond, suggesting the presence of peptide structure (Pelton and McLean, 2000). Meanwhile, 1H nuclear magnetic resonance (1H NMR) has been conducted to clearly

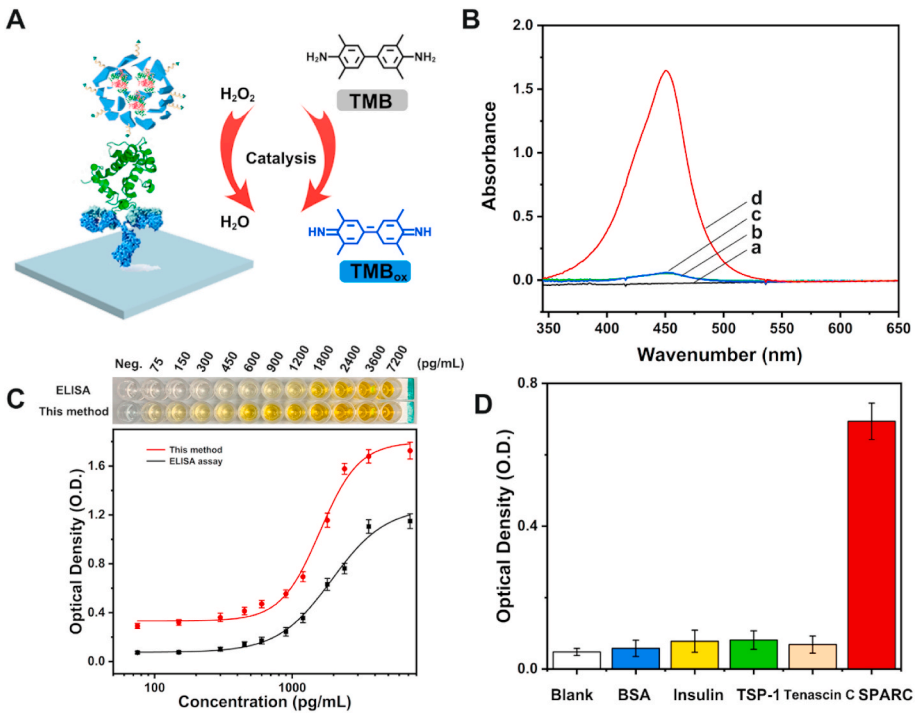

Fig. 4. (A) Schematic illustration for the detection of SPARC in a sandwich immunoassay. (B) The signal response of sandwich immunoassays using (a) TMB/H_2O_2, (b) SPARC + TMB/H_2O_2, (c) peptide-HRP@ZIF-90 + TMB/H_2O_2, and (d) SPARC + peptide-HRP@ZIF-90 + TMB/H_2O_2. The concentration of SPARC and peptide-HRP@ZIF-90 are 2400 pg/mL and 50 μg/mL, respectively. (C) Comparison of the detection performance between this assay and conventional ELISA by plotting absorption intensities at 450 nm versus various concentrations of SPARC. (D) The selectivity of this method. The concentrations of SPARC and other proteins are 1200 pg/mL and 1200 ng/mL, respectively. The error bars represent standard deviation from average (n = 3).

demonstrate the successful process of post-synthetic modification (Figs. S7–9). And, the loading ratio of peptide-HRP on the ZIF-90 is calculated to be about 5 wt % by the BCA Protein Assay Kit.

Additionally, we have measured the catalytic activity of peptide-HRP@ZIF-90 by tracking the color change of TMB with time via a measurement of absorbance at 650 nm. It can be observed that HRP@ZIF-90 can maintain a high catalytic activity after the surface is functionalized with peptides (Fig. S10), which means that the chain structure of peptides will not affect the interaction between immobilized enzymes and free substrates. Also, the rate of the enzymatic reaction increased as the concentration of biocatalyst increased under the same conditions (Fig. S11). Meanwhile, peptide-MOF demonstrates a negligible enzyme leaching (Fig. S12). Collectively, the peptide-HRP@ZIF-90 has been successfully prepared and characterized.

3.3. Feasibility of sensing method

We have further evaluated the recognition capability for subsequent unambiguous-detection and quantification. As illustrated in Fig. 4A, the target protein SPARC is first bound to the capture antibody. Then SPARC-binding peptide modified on the surface of HRP@ZIF-90 can specifically recognize target proteins, fabricating a classic "sandwich assay". After that, a series of control experiments have been conducted to validate the feasibility of this assay. As shown in Fig. 4B, the blank control group with the presence of TMB buffer exhibits no absorbance at 450 nm after the addition of stop buffer. Analogously, there is no obvious phenomenon in the two other groups added with protein targets or peptide-HRP@ZIF-90. However, only a complete detection system can be able to give a response signal, which proves that the nanocomposite has good molecular recognition ability, available to a working colorimetric assay for the detection of SPARC.

On the basis of the testing principle, we have optimized experimental conditions for the detection of SPARC by monitoring the colorimetric signals. Firstly, the concentration of HRP was optimized, because the amount of internal HRP determines the catalytic activity. As shown in Fig. S13A, with the increased concentrations of HRP, the signal intensity increases and reaches a plateau after 200 μg/mL. Secondly, since the distribution density of peptides on the surface of HRP@ZIF-90 may have impact on the recognition efficiency and diffusion of H_2O_2, the dose of peptides was optimized to a final concentration of 1 mg/mL during the process of surface functionalization (Fig. S13B). Then, the concentration of peptide-HRP@ZIF-90 and reaction time were optimized to 50 μg/mL and 15 min, respectively (Fig. S13C and Fig. S13D). Additionally, it can be observed that the responsive signal decreases significantly after 45 °C, with no difference from 25 °C to 37 °C, so the experiment were conducted at room temperature (Fig. S14A). And the best buffer has been optimized to be tris-citric acid buffer to obtain stable reaction environment (Fig. S14B). Thus, these conditions were employed in the following experiments.

3.4. Assay performance

To validate the detection performance, a contrast experiment on this assay and the commercially-available ELISA has been carried out. As shown in Fig. 4C, the two methods give different colorimetric response at the same concentration of targets. As expected, the detecting range of conventional ELISA assay is tested to be 300–3600 pg/mL (Fig. S15). However, with the concentration gradually decreasing, the ELISA assay generates negative response, while an obvious response can still be observed by using this method. It is reasonable, since ZIF-based bioassembly may increase the loading of HRP molecules to realize signal amplification. **What's more**, a linear relation of the OD value versus the concentration, ranging from 0.1 pg/mL to 1200 pg/mL, can be established (Fig. S16). The limit of detection is calculated to be 30 fg/mL, which is around 3000-fold lower than that of the ELISA assay.

In addition, control experiments by using bovine serum albumin (BSA), insulin, thrombospondin-1 (TSP-1), and tenascin have been conducted at the same conditions to evaluate the specificity of our method. Photograph in Fig. 4D shows that these proteins, even with 1000 times higher concentration, give negligible signal response. The strong interaction between peptide and SPARC guarantees the specificity of this method, validating the potential detectability of this strategy in complex samples.

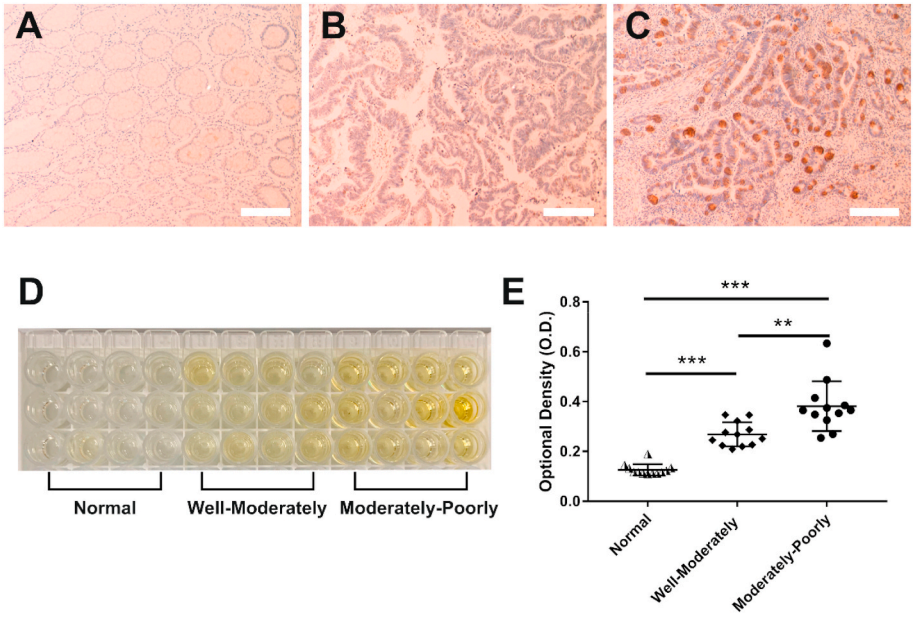

Fig. 5. Photographs of immunohistochemical analysis for colon cancer tissues with different degrees of differentiation, including (A) normal tissues around the cancer, (B) well-moderately differentiated issues, and (C) moderately-poorly differentiated issues. Scale bars = 200 μm. (D) The photograph of colorimetric responses toward three groups of tissue samples using this method. (E) The corresponding distribution of OD values. All spectra were obtained under 450 nm. Student's *t* test shows statistical significance: $^{**}P < 0.01$ and $^{***}P < 0.001$.

3.5. Analysis of clinical samples

We have also challenged this biosensor by detecting SPARC in real samples. It has been reported that the abnormal expression of SPARC plays an important role during the invasion and metastasis of human colon cancer (Naito et al., 2018; Yang et al., 2007). Therefore, 36 tissue samples from colon cancer patients have been collected from a local hospital. Informed consents are obtained in all cases, and the research is approved by the local scientific ethical committee. All samples are divided to 3 groups (normal tissues around the tumor, well-moderately differentiated issues, and moderately-poorly differentiated issues), 12 samples in each group, according to pathological diagnosis. Immunohistochemical analysis has also been conducted to determine the expression of SPARC in different issues. As shown in Fig. 5A–C, stained slices show that the result for normal group is negative, but the other two groups are positive. The samples are.

Prepared to be tissue lysates by extracting the total protein and quantified by BCA Protein Assay Kit. Under the same condition, 5 μL of lysates are diluted to 50 μL and added to the 96-well microplate. After the chromogenic reaction catalyzed by peptide-HRP@ZIF-90, the colorimetric responses of 36 samples are shown in Fig. 5D. Three distinct regions with different color shades can be observed in the microplate, which represents the normal group, the well-moderately differentiated group, and the moderately-poorly differentiated group (from left to right). The color gets darker with the decrease of differentiation level. Three groups of OD value data have been further statistically analyzed in Fig. 5E. Through Student's *t*-test, there is a very significant difference between cancerous group and normal group, and a significant difference between the two differentiated groups. It can be concluded that tissue expression of SPARC is positive correlation with the malignant degree of colon cancer, indicating the protein is closely related to the occurrence and development of colon cancer.

4. Conclusion

In summary, we have successfully prepared peptide-functionalized HRP@ZIF-90 nanocomposites for immunoassays of SPARC. The unique porous structure of the ZIF-90 may provide a stable protection framework for enzyme molecules, benefitting storage and transportation of the diagnostic reagents. The high loading of enzymes also ensures the signal amplification of this strategy in the detecting system, which allows sensitive detection at a pg mL^{-1} level. We have further demonstrated that the peptide-modified HRP@ZIF-90 nanocomposites can be used for the detection of SPARC in real samples with high accuracy. Moreover, the protein level of SPARC in colon cancer tissues with different differentiation degree has been determined, which may reveal the role of SPARC in the invasion and metastasis of human colon cancer. Certainly, the process of material synthesis needs to be further improved to ensure consistency among batches and larger sample populations are required to verify the clinical value of this new method. Nevertheless, this work has provided an alternative for the assay of SPARC. Meanwhile, the strategy proposed in this work can be used for other ZIFs with different enzymes and peptides, thereby greatly expanding their applications in the biomedical field.

CRediT authorship contribution statement

Shuai Wu: Conceptualization, Methodology, Software, Investigation, Validation, Data curation, Writing - original draft. **Zhaowei Sun:** Methodology, Investigation, Data curation. **Ying Peng:** Data curation, Validation. **Yiwei Han:** Software, Validation. **Jinlong Li:** Resources, Validation. **Sha Zhu:** Resources, Validation. **Yongmei Yin:** Validation, Supervision. **Genxi Li:** Funding acquisition, Supervision, Writing - review & editing.

Declaration of competing interest

The authors declare that they have no known competing financial interests or personal relationships that could have appeared to influence the work reported in this paper.

Acknowledgements

This work is supported by the National Natural Science Foundation of China (Grant Nos. 81772593, 21235003).

Appendix A. Supplementary data

Supplementary data to this article can be found online at https://doi.org/10.1016/j.bios.2020.112613.

References

Abazari, R., Ataei, F., Morsali, A., Slawin, A.M.Z., C, L.C.-W., 2019a. Acs Appl. Mater. Int. 11, 45442–45454.
Abazari, R., Morsali, A., Dubal, D.P., 2020. Inorg. Chem. Front. 7, 2287–2304.
Abazari, R., Sanati, S., Morsali, A., Slawin, A.M.Z., Carpenter-Warren, C.L., Chen, W., Zheng, A., 2019b. J. Mater. Chem. A 7, 11953–11966.
Bornstein, P., Sage, E.H., 2002. Curr. Opin. Cell Biol. 14, 608–616.
Chen, G., Kou, X., Huang, S., Tong, L., Shen, Y., Zhu, W., Zhu, F., Ouyang, G., 2020. Angew. Chem. Int. Ed. 59, 2867–2874.
Clark, C.J., Sage, E.H., 2008. J. Cell. Biochem. 104, 721–732.
Drout, R.J., Robison, L., Farha, O.K., 2019. Coord. Chem. Rev. 381, 151–160.
Gao, Z., Lv, S., Xu, M., Tang, D., 2017a. Analyst 142, 911–917.
Gao, Z., Xu, M., Lu, M., Chen, G., Tang, D., 2015. Biosens. Bioelectron. 70, 194–201.
Gao, Z., Ye, H., Tang, D., Tao, J., Habibi, S., Minerick, A., Tang, D., Xia, X., 2017b. Nano Lett. 17, 5572–5579.
Ghosh, D., Lee, Y., Thomas, S., Kohli, A.G., Yun, D.S., Belcher, A.M., Kelly, K.A., 2012. Nat. Nanotechnol. 7, 677–682.
Gimenez-Marques, M., Hidalgo, T., Serre, C., Horcajada, P., 2016. Coord. Chem. Rev. 307, 342–360.
Hanahan, D., Weinberg, R.A., 2000. Cell 100, 57–70.
Hanahan, D., Weinberg, R.A., 2011. Cell 144, 646–674.
Horcajada, P., Gref, R., Baati, T., Allan, P.K., Maurin, G., Couvreur, P., Ferey, G., Morris, R.E., Serre, C., 2012. Chem. Rev. 112, 1232–1268.
Huang, S., Kou, X., Shen, J., Chen, G., Ouyang, G., 2020. Angew. Chem. Int. Ed. 59, 8786–8798.
Joyce, J.A., Pollard, J.W., 2009. Nat. Rev. Canc. 9, 239–252.
Junttila, M.R., de Sauvage, F.J., 2013. Nature 501, 346–354.
Kelly, K.A., Waterman, P., Weissleder, R., 2006. Neoplasia 8, 1011–1018.
Kou, X., Tong, L., Shen, Y., Zhu, W., Yin, L., Huang, S., Zhu, F., Chen, G., Ouyang, G., 2020. Biosens. Bioelectron. 156, 112095.
Li, J.R., Kuppler, R.J., Zhou, H.C., 2009. Chem. Soc. Rev. 38, 1477–1504.
Lian, X.Z., Fang, Y., Joseph, E., Wang, Q., Li, J.L., Banerjee, S., Lollar, C., Wang, X., Zhou, H.C., 2017. Chem. Soc. Rev. 46, 3386–3401.
Liang, K., Ricco, R., Doherty, C.M., Styles, M.J., Bell, S., Kirby, N., Mudie, S., Haylock, D., Hill, A.J., Doonan, C.J., Falcaro, P., 2015. Nat. Commun. 6, 7240.
Liang, W.B., Xu, H.S., Carraro, F., Maddigan, N.K., Li, Q.W., Bell, S.G., Huang, D.M., Tarzia, A., Solomon, M.B., Amenitsch, H., Vaccari, L., Sumby, C.J., Falcaro, P., Doonan, C.J., 2019. J. Am. Chem. Soc. 141, 2348–2355.
Liu, Y.P., Hsiao, M., 2013. Gut 62, 810–811.
Ma, J., Gao, S., Xie, X., Sun, E., Zhang, M., Zhou, Q., Lu, C., 2017. Oncol. Lett. 14, 5876–5882.
Morris, W., Doonan, C.J., Furukawa, H., Banerjee, R., Yaghi, O.M., 2008. J. Am. Chem. Soc. 130, 12626.
Naito, T., Kitadai, Y., Takigawa, H., Yuge, R., Kuwai, T., Yasui, W., Tanaka, S., Chayama, K., 2018. Canc. Sci. 109, 1029-1029.
Papapanagiotou, A., Sgourakis, G., Karkoulias, K., Raptis, D., Parkin, E., Brotzakis, P., Panchal, S., Papavassiliou, A.G., 2018. J. Int. Med. Res. 46, 2769–2779.
Pelton, J.T., McLean, L.R., 2000. Anal. Biochem. 277, 167–176.
Quail, D.F., Joyce, J.A., 2013. Nat. Med. 19, 1423–1437.
Said, N.A., Elmarakby, A.A., Imig, J.D., Fulton, D.J., Motamed, K., 2008. Neoplasia 10, 1092–1104.
Sanati, S., Abazari, R., Morsali, A., 2020. Chem. Commun. 56, 6652–6655.
Sanati, S., Abazari, R., Morsali, A., Kirillov, A.M., Junk, P.C., Wang, J., 2019. Inorg. Chem. 58, 16100–16111.
Shieh, F.K., Wang, S.C., Yen, C.I., Wu, C.C., Dutta, S., Chou, L.Y., Morabito, J.V., Hu, P., Hsu, M.H., Wu, K.C.W., Tsung, C.K., 2015. J. Am. Chem. Soc. 137, 4276–4279.
Tichet, M., Prod'Homme, V., Fenouille, N., Ambrosetti, D., Mallavialle, A., Cerezo, M., Ohanna, M., Audebert, S., Rocchi, S., Giacchero, D., Boukari, F., Allegra, M., Chambard, J.C., Lacour, J.P., Michiels, J.F., Borg, J.P., Deckert, M., Tartare-Deckert, S., 2015. Nat. Commun. 6, 6993.
Veitch, N.C., 2004. Phytochemistry 65, 249–259.
Wei, T.H., Wu, S.H., Huang, Y.D., Lo, W.S., Williams, B.P., Chen, S.Y., Yang, H.C., Hsu, Y. S., Lin, Z.Y., Chen, X.H., Kuo, P.E., Chou, L.Y., Tsung, C.K., Shieh, F.K., 2019. Nat. Commun. 10, 5002.
Wong, G.S., Rustgi, A.K., 2013. Br. J. Canc. 108, 755–761.
Yang, E., Kang, H.J., Koh, K.H., Rhee, H., Kim, N.K., Kim, H., 2007. Int. J. Canc. 121, 567–575.
Yang, T., Chung, T.-S., 2013. J. Mater. Chem. A 1, 6081–6090.
Zhang, F.M., Dong, H., Zhang, X., Sun, X.J., Liu, M., Yang, D.D., Liu, X., Wei, J.Z., 2017. Acs Appl. Mater. Int. 9, 27332–27337.